DOI: 10.37190/ABB-02380-2024-04

Biomechanical Assessment of Lumbar Stability: Finite Element Analysis of TLIF with a Novel Combination of Coflex, and Pedicle Screws

S Meganathan[1], M. S. Alphin[1*]

[1]Department of Mechanical Engineering, Sri Sivasubramaniya Nadar College of Engineering, Kalavakkam, Chennai– 603110, India

[*]Corresponding author: M. S. Alphin, Department of Mechanical Engineering, Sri Sivasubramaniya Nadar College of Engineering, Kalavakkam, Chennai, Tamilnadu, India, e-mail address: AlphinMS@ssn.edu.in

Submitted: 11th January 2024

Accepted: 20th March 2024

Abstract

Purpose: Finite element analysis is frequently used for lumbar spine biomechanical analysis. The primary scope of this work is to illustrate, using finite element analysis, how the biomechanical behavior of the Transforaminal lumbar Interbody fusion (TLIF), along with a novel combination of the Interspinous process device (IPD) and pedicle screws, improves lumbar spine stability.

Methods: In this study, Unilateral Pedicle Screw Fixation (UPSF) and Bilateral Pedicle Screw Fixation (BPSF) were used. Four FE model was developed using ANSYS software, as follows: (1) Intact model; (2) TLIF with "U"-shaped Coflex-F IPD (UCF); (3) TLIF with Coflex-F and UPSF (UCF + UPSF); and (4) TLIF with Coflex-F and BPSF (UCF + BPSF). The intact model was subjected to four pure moments (10 Nm), and the results were validated with previous literature data. The intact model results correlated well with the literature data, and the model was validated. Three surgical models were subjected to 7.5 Nm four pure moments, Flexion (FL), Extension (ET), Lateral bending (LB), and Axial rotation (AR) and a 280N follower load.

Results: The surgical model results are compared with the intact model. The comprehensive analysis results show the UCF + BPSF surgical model gave a good advantage on range of motion, cage stress, Coflex-F stress, and endplate stress compared among the two models.

Conclusion: This study proposes that the UCF + BPSF system helps to reduce the stress on the implant and adjacent endplates and gives very good stability to the lumbar spine under the various static loading conditions.

Keywords: Finite element analysis, Lumbar, Biomechanics, TLIF, Pedicle Screws, Biomaterials.

Abbreviations

TLIF - Transforaminal Lumbar Interbody Fusion

IPD - Interspinous Process Device

UPSF - Unilateral Pedicle Screw Fixation

BPSF - Bilateral Pedicle Screw Fixation

FE - Finite Element

UCF - TLIF with "U"-shaped Coflex-F IPD

UCF + UPSF - TLIF with Coflex-F and UPSF
UCF + BPSF - TLIF with Coflex-F and BPSF
IVD - Intervertebral Disc
L - Lumbar vertebral bodies
CT - Computed Tomography
N - nucleus pulposus
ROM – Range of Motion
Mvms - Maximum von mises stress
FL – Flexion, ET – Extension, LB – Lateral Bending, AR – Axial Rotation

1. Introduction

TLIF is a commonly using surgical procedure for addressing the lower back pain in a long-term situation [22]. One of its main advantages is its ability to reduce neurological complications while still allowing the use of a comparatively large Interbody cage via a small incision [17],[47]. However, it is essential to understand that traditional pedicle screw fixation systems have limitations. UPSF, BPSF are the two common type of Pedicle Screw system. It increases motion and stress in the adjacent spinal segments, resulting in adjacent spinal degeneration over time [11],[33].

Long-term complications of the Pedicle Screw system include screw misalignment, pedicle breakage, loss of correction, and screw loosening [33]. These challenges increase the demand for surgical technique advancements. According to biomechanical studies, the pedicle screw system may cause stress concentrations, particularly in the center regions of the rods and the neck portion of the screws [11]. This highlights the importance of improving the design and application of pedicle screw fixation to reduce biomechanical stress and its possible adverse effects. Based on these considerations, additional research and development are required to improve the effectiveness of TLIF procedures, particularly pedicle screw fixation procedure [42].

Surgeons are currently looking into the use of IPDs, as a less invasive procedure that can replace lumbar fusions [23]. IPDs provides relief from pressure on the canal of the spinal cord and nerve roots by creating space in between the intervertebral bodies [12], [38]. The advantage of IPDs over traditional pedicle screw fixation is that they produce comparable clinical and radiologic results while reducing surgery times, blood loss, and hospitalizations [34],[39]. The Coflex-F IPD has been created to assist in fusion surgeries [47]. According to studies, it is effective at stabilizing the surgical area, particularly during flexion, and bending motion. Researchers compared its biomechanical behavior with the characteristics of other fusion methods such as Posterior Lumbar Interbody Fusion and Anterior Lumbar Interbody Fusion [9],[10].

Despite its potential to provide a balance of stabilization and fusion, research suggests that the UCF has some limitations [22],[33],[47]. These limitations include the level and effectiveness of fusion achieved, the biomechanical interaction between the techniques, and the variability in clinical outcomes observed among patients. Understanding these limitations is critical in order to select the best surgical approach for each individual's unique spinal condition. Comprehensive literatures shows that IPD and Pedicle Screw systems not significantly provide stability to all kind of motions with TLIF procedure, it has some limitation both stabilization systems [9],[10].

In order to fill these gaps, a new study has been initiated to investigate the biomechanical behavior of UCF and Pedicle Screw systems. The purpose of this research study is to investigate how the UCF and Pedicle Screw systems improves biomechanical behavior under static loading conditions.

2. Material and Methods

2.1. Development of Lumbar FE - model.

The lumbar spine FE - model was constructed using Computed Tomography (CT) Scan Images of a 32 year old healthy female volunteer with no prior medical history of spine injury or degeneration. The CT scan images were used after the volunteer expressed concern. Creating an FE model that includes the exact dimensions of the lumbar spine and internal structures is critical for biomechanical investigations [14],[28]. In this investigation, general and effective methods were applied.

The CT scan images are imported in DICOM file format into the MIMICS 14.0 software (Materialize, Leuven, Belgium) [25]. To obtain the masks of the intervertebral disc (IVD) and Lumbar vertebral bodies (L1-L5), MIMICS 14.0 used threshold segmentation based on the CT data. Extraction of the solid lumbar spine model and export as a Standard Triangle Language (STL) file are accomplished through the use of the masking technique. After that, the STL file was imported into Geomagic Studio 12.0 (3D Systems, South Carolina, and USA) to perform geometric smoothing and cleanup [4]. Furthermore, the processed 3D model was imported into Space Claim software (ANSYS.Inc, Canonsburg, Pennsylvania, United States) for the creation of an intervertebral body, endplate, and nucleus pulposus (N1-N5).

Then using Boolean operation surgical implant cage of TLIF was added to the Lumbar Model [29]. One intact model and three surgical models, totally four models created for this analysis; (1) Intact, (2) UCF, (3) UCF + UPSF, (4) UCF + BPSF is shown in Figure 1(a-d). The prior research provides a detailed description of the lumbar spine analysis process [31],[42].

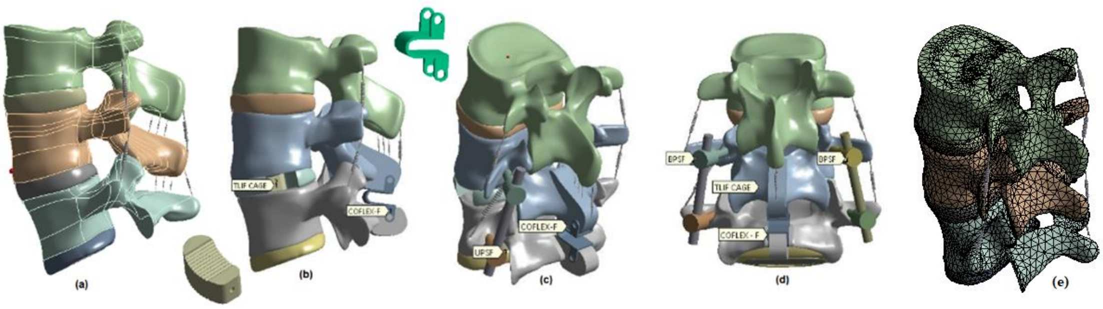

Figure 1. (a) Intact Lumbar model, (b) Lumbar (L4-L5) surgical model with TLIF implant and Coflex (UCF), (c) Lumbar (L4-L5) surgical model with TLIF implant, Coflex and UPSF (UCF + UPSF), (d) Lumbar (L4-L5) surgical model with TLIF implant, Coflex and BPSF (UCF + BPSF), (e) Intact lumbar model (Meshed View)

Table.1: Material property of lumbar spine FE model various parts with its values.

Part Name	**Young's Modulus Value (MPa)**	**Poisson Ratio**	**Cross Section Area (mm^2)**	**Density (Kg/mm^3)**	**References**
Cortical Bone	12,000	0.3	--	1.70×10^{-06}	[27]
Cancellous Bone	100	0.2	--	1.10×10^{-06}	[8]
Posterior Bone	3500	0.25	--	1.40×10^{-06}	[3]
Endplate	24	0.25	--	1.20×10^{-06}	

nucleus_pulposus	1	0.49	--	1.02×10^{-06}	
Annulus Fibrosus	4.2	0.45	--	1.05×10^{-06}	[15]
Anterior Longitudinal Ligament (ALL)	20	0.3	63.7	1.00×10^{-06}	
Posterior Longitudinal Ligament (PLL)	20	0.3	20	1.00×10^{-06}	[37],[47]
Ligament Flava (LF)	19.5	0.3	40	1.00×10^{-06}	[5]
Interspinal Ligament (ISL)	11.6	0.3	40	1.00×10^{-06}	
Supraspinal Ligament (SSL)	15	0.3	30	1.00×10^{-06}	
Intertransverse Ligament (ITL)	58.7	0.3	3.6	1.00×10^{-06}	
Pedicle screws (Titanium)	110,000	0.3	--	4.50×10^{-06}	
Coflex (Titanium)	110,000	0.3	--	4.50×10^{-06}	
Cage (Titanium)	110,000	0.3	--	4.50×10^{-06}	

The main focus of this analysis is on the biomechanical behaviors of L4-L5. To reduce the computational time, the L1-L5 is simplified to L3-L5 [30]. The material property of the lumbar is shown in Table.1. The ligaments are created by using a spring unit (Tension load only) and the property of Ligament stiffness as shown in Table.2.

The contact between the bone and IVD is considered as boned contact [7] with Multi Point Constraint contact formulation and contact between two cartilages is frictional contact with a frictional coefficient value of 0.2 [20]. The frictional contact is created by the pure penalty formulation method. The following steps are done to avoid the meshing error. Tet Mesh is utilized for all elements of the lumbar model to speed up and simplify the meshing process. The meshing size for the individual parts and no of nodes of each part of the model as shown in the Table 3. The process of meshing carried out with acceptable nodes and elements count.

Table 2 Stiffness of Ligaments in N-mm [13]

Ligaments	**ALL**	**PLL**	**ISL**	**SSL**	**LF**	**ITL**
L3-L4	40 ± 20	10.5 ± 8	18.1 ± 16	35 ± 11.7	35 ± 6.2	50
L4-L5	40.5 ± 14	25.8 ± 16	8.7 ± 6.5	18 ± 6.8	27.1 ± 12	50

Table.3. Individual meshing properties of the lumbar spine model

Parts	Element size (mm)	Element name	Node count	Element count	References
L3	3	10 node Tet element	20136	12065	
L4	3	10 node Tet element	21280	12759	
L5	3	10 node Tet element	18220	10882	
IVD3	2	10 node Tet element	13902	8117	
IVD4	2	10 node Tet element	12441	7199	[6],[13],[35]
IVD5	2	10 node Tet element	11910	6851	
N3	2	10 node Tet element	8679	5183	
N4	2	10 node Tet element	7309	4328	
N5	2	10 node Tet element	5945	3433	

2.2. Boundary conditions

The boundary conditions are applied with two different conditions, (1) Intact lumbar model (2) Surgical lumbar model. The L5 lumbar vertebra's lower surface was validated to remain stationary using a rigid constraint with six degrees of freedom in both models. It does not experience displacement or rotation when subjected to a moment. This constraint is consistent with the methodology used in previous research [3]-[5],[8],[15],[21],[27]-[31]. There were two load conditions used. The initial load conditions were designed to validate the Intact of the finite element (FE) model. L5's inferior surface was fixed in all directions to ensure stability [46].

Figure 2 (a) shows the boundary condition for the intact, at the center of the L3 superior surface, pure moments of 10 Nm in flexion (FL), extension (ET), lateral bending (LB), and axial rotational (AR) were then applied. Additionally, the IVD stress and axial displacement of L4-L5 were compared to prior experimental research by progressively increasing the preload values (100N, 200N, 300N, and 400 N) on the lumbar model [1].

The second loading condition was applied both intact and surgical models. A 7.5 Nm moment was applied to the L3 superior surface to simulate four motions such as flexion, extension, lateral bending, and axial rotation [18]. In addition, a bilateral set of connector elements applied a 280 N follower load along the curvature of the lumbar spine, representing partial body weight [47]. In the case of surgical models, displacement control was used to achieve the same L3-L5 range of motion as the intact model. Finally, the calculations included determining the range of motion (ROM) and intervertebral disc pressure.

3. Results

3.1. Intact model results

3.1.1. Verification of IVD3 - ROM

The IVD3 of intact model was validated with previous experimental results. The deformation of intact lumbar model under the four motions are shown in Figure 2(c).

3.1.2. Calculation of ROM

The rotational angle of L3 & L4 for the intact model is shown in Figure 2(b) [47].

Range of motion of IVD3 = Angle of rotation of L3 – Angle of rotation of L4

$$= 6.0199 - 2.45315 = 3.56675$$

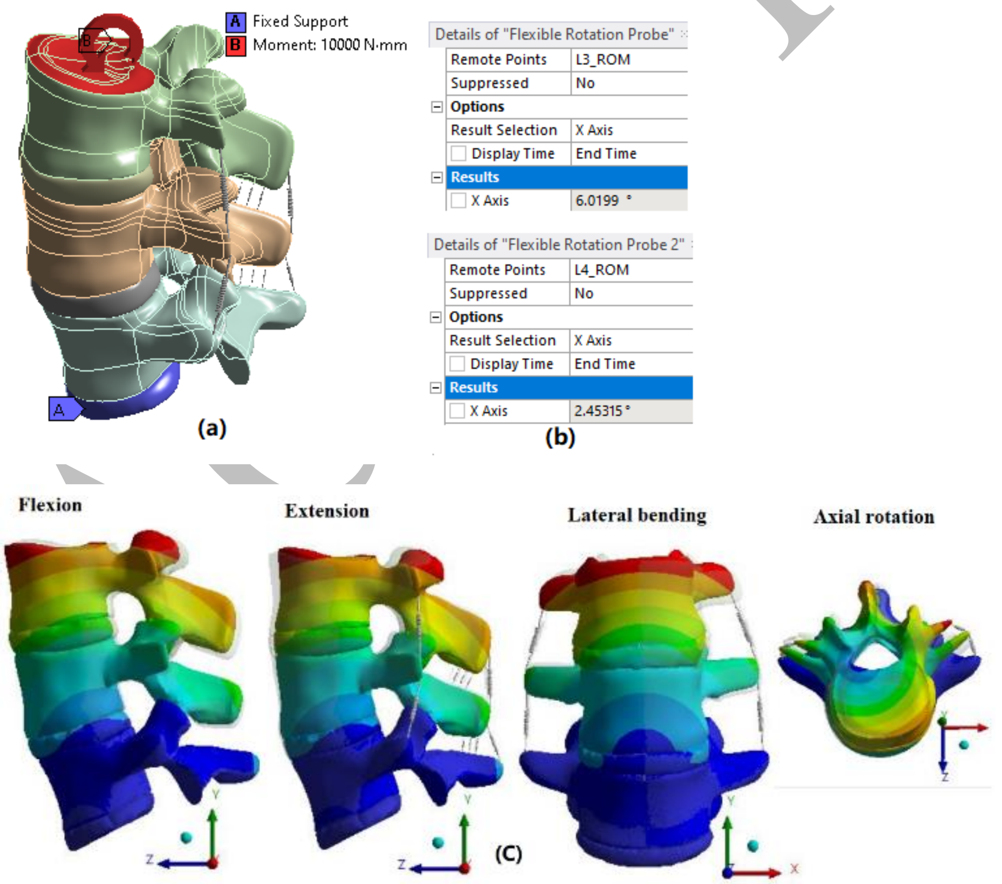

Figure 2. (a) Boundary conditions – Intact Model, (b) Angle of rotation of L3 & L4 calculated by ANSYS software. (c) Intact lumbar model deformation plot for four pure moment (10 Nm).

The graphical representation of the ROM of the IVD3 compared with various previous literature review [2],[41],[25] is shown in Figure 3(a). The Intact lumbar model is simplified to L3-L5 because of the scope of the present study only considering the L4-L5. The results shows the present Intact FE model is reliable and valid.

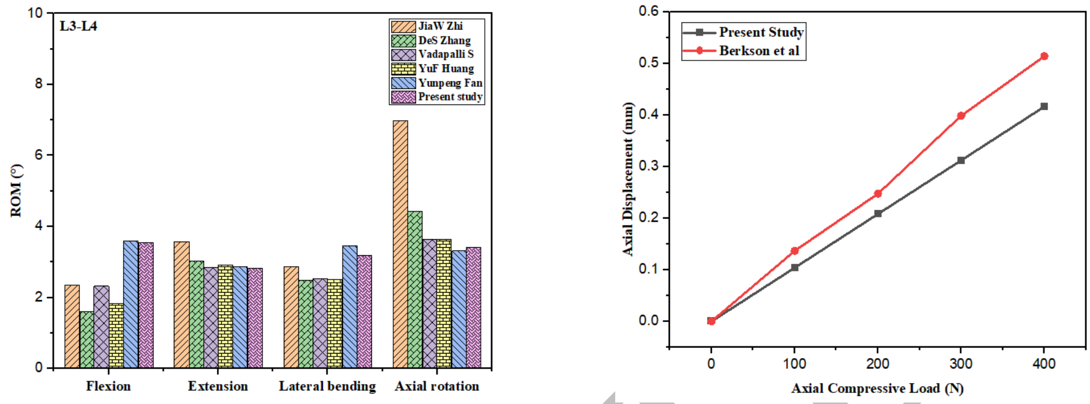

(a) (b)

Figure 3. (a) ROM of Intact lumbar spine model (L3-L4) compared with other literature data. (b) Load Vs Displacement of the present FE model (L4 - L5) with Berkson et al.

3.1.3. Verification of Axial displacement:

The axial displacement of the IVD of intact model (L4-L5) with respect to the increased load as shown in Figure 3(b). The result of load versus displacement is compared with Berkson et al [2]. The results are accordance with the literature review data. It shows the present FE model is valid and reliable.

3.1.4. Verification of Von Mises stress of IVD3

The maximum von mises stress (Mvms) of IVD3 in the intact model is compared with previous literature reviews [13],[40],[41],[44]. The results are shown in Figure 4 is comparatively accordance with the literature review data. Therefore, the current intact FE model proved to be valid and reliable.

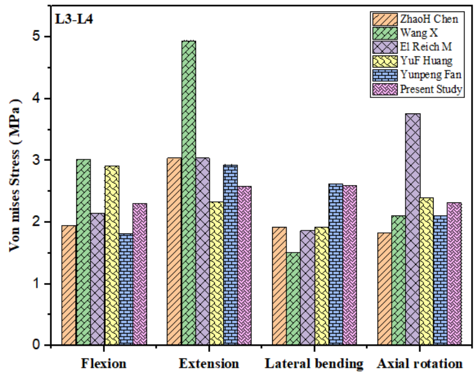

Figure 4. Comparison of Intact model Mvms (L3-L4) under four pure moment (10 Nm) with literature review data.

3.2. Results of surgical model

3.2.1. ROM of Intact vs surgical model.

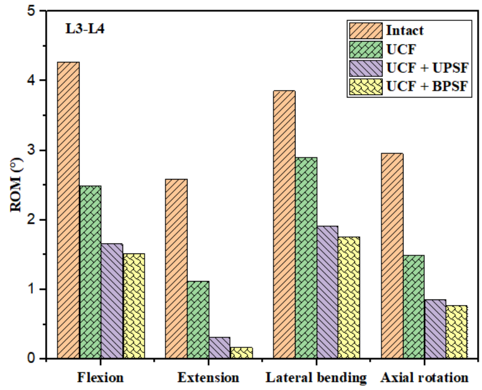

Figure 5. Comparison of Surgical mode with Intact model ROM (L3-L4) under four pure moment (7.5 Nm) with follower load (280N).

The lumbar spine surgical model with expected range of motion under static loading conditions is shown in Figure 5. When compared to an intact model, the TLIF procedure significantly decreased the ROM in all motion conditions. It's clearly shows that the UCF + BPSF provides good stability and has the lowest ROM when compared to all other models. Compare with intact model, the UCF + BPSF ROM decreased significantly to 64% in FL, 93% in ET, 54% in LB, and 74% in AR. Furthermore, the ROM of the UCF model by itself is 42%, 57%, 25%, and 49%, respectively. Also, the UCF + UPSF's ROM is 61%, 88%, 50%, and 71%, respectively. Under all motion conditions, the UCF + BPSF model has the less amount of ROM motion. Compared to UCF, UCF+UPSF have less

ROM in all the motion. The ROM of L3-L4 calculated by L3 angle of rotation minus L4 angle of rotation.

3.2.2. Maximum Von mises Stress

The Maximum Von mises Stress (Mvms) of IVD L3-L4 surgical model is shown in Figure 6(a), and 7(a). It clearly shows that minimum von mises stress in the axial rotation motion compare to all other motion. The UCF+BPSF surgical model had maximum stress value (1.073 MPa) in extension motion and minimum (0.240 MPa) in axial rotation of intact model. Additionally, UCF + BPSF model showed higher stress in all motions as compared to UCF + UPSF model. Compared with UCF + UPSF model, the UCF model is high stress in all motions. Similarly the Mvms of L5-Sacrum has higher stress than L3-L4 is shown in Figure 6(b).

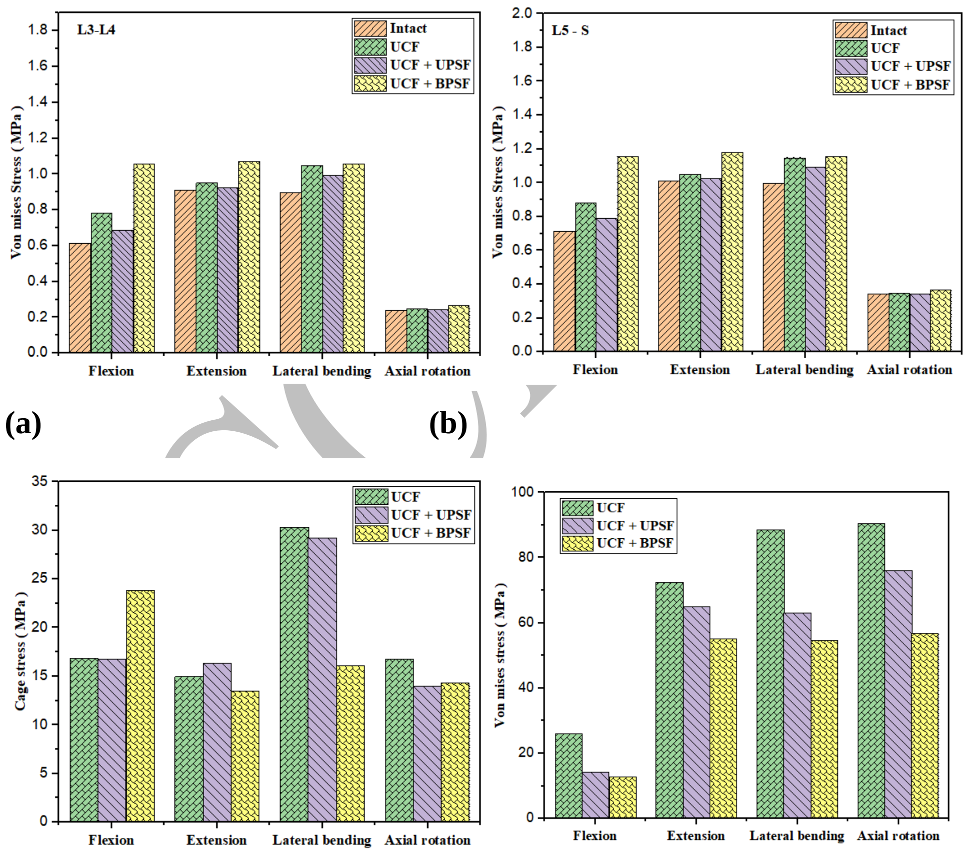

(a) (b)

(c) (d)

Figure 6. Comparison of Maximum vonmises stress of : (a) IVD (L3-L4), (b) IVD (L5-S) (c) Implant Cage, (d) Coflex- F IPD

In this analysis, surgical model analyzed under four motion conditions. The Mvms of cage under various motion for the three surgical models is shown in Figure 6(c) & 7(b). It shows the UCF had the Mvms (30 MPa) in LB motion compare to all other models. Also UCF + BPSF model had minimum von mises stress (13.5 MPa) in the ET motion. The highest von mises stress experienced during lateral bending relative to all other motions. In ET motion, UCF + UPSF exhibited noticeably higher von mises stress than other models.

In this investigation, TLIF cages with UCF were implanted in all surgery models. Three surgical models were analyzed under four motions. The MVMS for UCF is shown in Figure 6. (d), 7(c). It clearly shows the MVMS at UCF model under axial rotation motion. The minimum stress at UCF + BPSF model in flexion motion. UCF model comparatively higher stress in all motions. In every motion, UCF + UPSF exhibited noticeably higher von mises stress than UCF + BPSF, according to the comparison of both UCF stress.

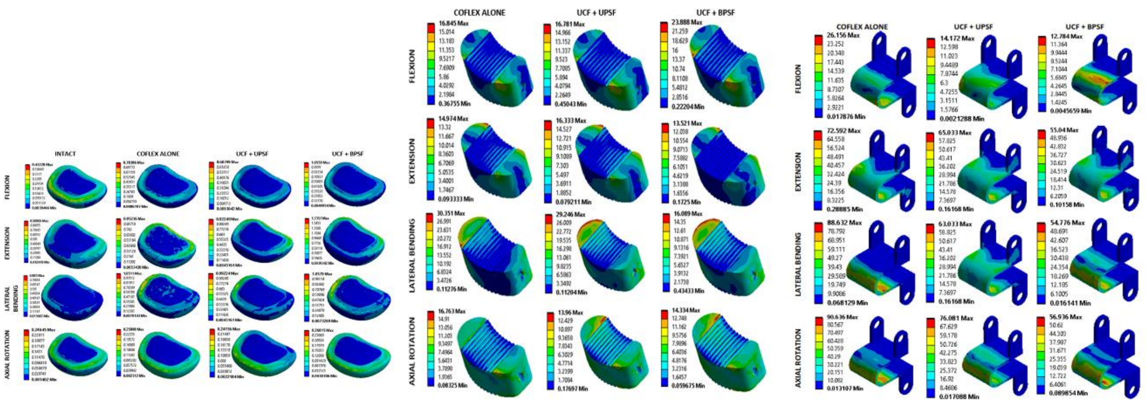

(a) (b) (c)

Figure 7. Contour plot of Maximum vonmises stress for: (a) IVD (L3-L4), (b) Implant Cage (c) Coflex- F IPD

The end plate stress is the important parameter for the measuring the biomechanical behavior of the spine. Figures 8 (a), (b), and (c) shows comparison of L4 inferior end plate and L5 superior end plate stresses for all surgical and intact model under static loading.

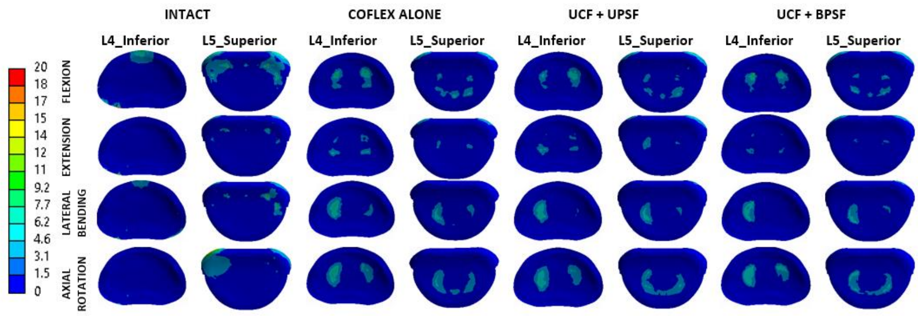

(a)

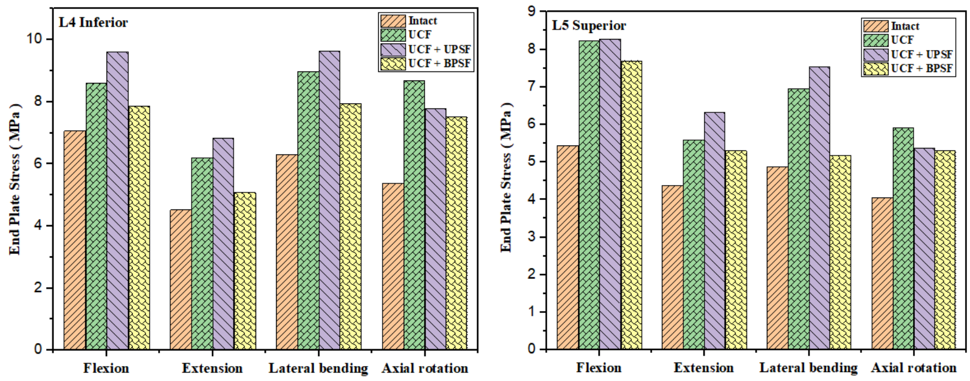

(b) **(c)**

Figure 8. (a) Contour plot of Maximum vonmises stress for L4 inferior and L5 superior end plates (b) Comparison of Maximum vonmises stress of L4 inferior end plate (c) Comparison of Maximum vonmises stress of L5 inferior end plate.

Table .4. Overall comparison of surgical model under static loading condition

Overall comparison of biomechanical performance in surgical model under static loading condition					
ROM	UCF alone	>	UCF+UPSF	>	UCF+BPSF
IVD stress	UCF+BPSF	>	UCF+UPSF	≈	UCF alone
Cage stress	UCF+UPSF	≈	UCF alone	>	UCF+BPSF
UCF stress	UCF alone	>	UCF+UPSF	>	UCF+BPSF
End Plate stress	UCF+UPSF	≈	UCF alone	>	UCF+BPSF

In the L4 inferior endplate at UCF + UPSF model significantly higher stress in FL, ET, and LB except axial rotation. Compared to UCF+BPSF, UCF+UPSF have slightly high stress in FL, ET, and AR except LB. In the L5 superior endplate stress at all the surgical models have significantly high stress compared to intact model. The UCF alone model and UCF+UPSF model have equal stress in flexion. UCF+BPSF, significantly high stress compared to Coflex alone and UCF+UPSF in LB and AR. In flexion and extension it's vice versa.

4. Discussion

The Prior research have shown that IPDs have shown positive results over the short and long terms [19],[26],[32]. In this investigation, FE models were subjected to four moment loading conditions. Although UPSF have very good advantages on tissue disruption, less blood loss procedure, and the operation time is less, but several biomechanical investigations have suggested that this technique is significantly less stable than BPSF due to the only one side fixation point cause asymmetric effect [45].

The current study shows the similar trends in ROM of surgical models with intact model. Compared to UCF model, the both UCF + UPSF and UCF + BPSF models have less in ROM. It happens because of the UPSF and BPSF restrict the motion of the adjacent lumbar [24]. The Coflex-F device and TLIF model exhibited less stability, particularly when it came to axial rotation and lateral bending in both directions [22]. In current study also UCF alone surgical model have maximum ROM compared to all other model, which shows the instability of UCF model on lumbar spine. The overall biomechanical behavior of surgical models as shown in Table.4. The TLIF procedure, slightly raised the stress in the adjacent IVD's. The Figure 6(a) and (b) shows that, stress of IVD5 (between the L5 and sacrum(S)) is higher than the IVD3 (between the L3- L4). The implant cage transfer the load to the adjacent IVD, which increase the stress in the IVD5 [16].

The UCF alone model allows motions compared to the other two surgical models. Which increase load on the implant cage, correspondingly the stress is increased in UCF model compared to the three surgical models cage stress is shown in Figure 6(d) & 7(c).[43] UCF alone model has high Mvms in lateral bending motion. UCF model comparatively higher stress in all motions. In every motion, UCF + UPSF exhibited noticeably higher von mises stress than UCF + BPSF, according to the comparison of both IPD stress. A comprehensive analysis of all the parameters (Table.4) shows that UCF + BPSF model has improved ROM and stability over the lumbar, IPD and cage.

Despite the fact that surgical models have their own advantages, they do have limitations. Because this study only included one unique person's data, the results do not represent the average number of people in the study. Although the lumbar materials in real life have nonlinear material properties, the material used in this analysis is linear elastic. In spite of this, the outcomes won't alter much [47]. Furthermore, the applied follower load does not have an adverse effect on the lumbar region. Moreover, the degeneration characteristics were not included in the analysis. The overall results shows, the UCF + BPSF model have good lumbar stability and minimum stress on Coflex, Implant cage, and end plates.

4.1. Limitations

The primary understanding of this FE study limited it to static structural analysis. Future research can include additional dynamic loading, such as vibration loading and friction between the facet joints. Also in this study assumed that the material properties of the lumbar spine and other parts were considered as linear elastic behavior [47], but in reality its nonlinear behavior. Despite of that, the predicted results would not significantly changed with the literatures. In spite of this, the expected outcomes would not materially alter based on the literature. This study's FE model does not account for spondylolisthesis, IVD collapsed height, or spine degeneration diseases. The results of this study, which only employed one distinct FE model, might not be typical of the general population.

5. Conclusion

In this study, the novel combination of Interspinous Process Device and Pedicle Screws used to create three surgical conditions UCF alone, UCF + UPSF, and UCF + BPSF were used to examine the biomechanical behaviors of the TLIF procedure under static loading conditions. Despite of the surgical models has its own advantages and limitation. Compared all the surgical models, UCF + BPSF model has very good advantage over the cage, IPD, end plate, ROM and stability. Introducing the UCF with pedicle screws are provides good advantageous in clinical practice. It will reduce the patients risk in long term journey.

Acknowledgement

We are grateful to everyone who supported our research and assisted in solving the issues. There was no funding obtained for this research.

Declaration of conflicting interests

All authors declare no competing interests.

References

[1] Araújo ÂRG., Peixinho N., Pinho ACM., Claro JCP. Quasi-static and dynamic properties of the intervertebral disc: Experimental study and model parameter determination for the porcine lumbar motion segment. Acta Bioeng Biomech 2015; 17(4): 59–66. Doi: 10.5277/ABB-00153-2014-04.

[2] Berkson MH., Nachemson AL., Nachemson A., Schultz AB., Schultz AB. Mechanical Properties of Human Lumbar Spine Motion Segments—Part II: Responses in Compression and Shear; Influence of Gross Morphology. Journal of Biomechanical Engineering-Transactions of The Asme 1979. Doi: 10.1115/1.3426225.

[3] Cai X yi., Sun M si., Huang Y peng., Liu Z xuan., Liu C jie., Du C fei., Yang Q. Biomechanical Effect of L4–L5 Intervertebral Disc Degeneration on the Lower Lumbar Spine: A Finite Element Study. Orthop Surg 2020; 12(3): 917–30. Doi: 10.1111/os.12703.

[4] Calişal E., Uğur L. Evaluation of the plate location used in clavicle fractures during shoulder abduction and flexion movements: A finite element analysis. Acta Bioeng Biomech 2018; 20(4): 41–6. Doi: 10.5277/ABB-01211-2018-03.

[5] Chen SH., Lin SC., Tsai WC., Wang CW., Chao SH. Biomechanical comparison of unilateral and bilateral pedicle screws fixation for transforaminal lumbar interbody fusion after decompressive surgery - A finite element analysis. BMC Musculoskelet Disord 2012; 13. Doi: 10.1186/1471-2474-13-72.

[6] Chen SH., Tai CL., Lin CY., Hsieh PH., Chen WP. Biomechanical comparison of a new stand-alone anterior lumbar interbody fusion cage with established fixation techniques - A three-dimensional finite element analysis. BMC Musculoskelet Disord 2008; 9. Doi: 10.1186/1471-2474-9-88.

[7] Chen S-I., Lin R-M., Chang C-H. Biomechanical investigation of pedicle screw–vertebrae complex: a finite element approach using bonded and contact interface conditions. Med Eng Phys 2003; 25(4): 275–82. Doi: https://doi.org/10.1016/S1350-4533(02)00219-9.

[8] Fan W., 2018 LGPU-. A comparison of the influence of three different lumbar interbody fusion approaches on stress in the pedicle screw fixation system: Finite element static and vibration analyses. Int J Numer Method Biomed Eng n.d. Doi: https://doi.org/10.1002/cnm.3162.

[9] Fan W., 2019 LGPU-. Biomechanical comparison of the effects of anterior, posterior and transforaminal lumbar interbody fusion on vibration characteristics of the human lumbar spine. Comput Methods Biomech Biomed Engin n.d. Doi: https://doi.org/10.1080/10255842.2019.1566816.

[10] Fan W., 2020 LGPU-. The effect of non-fusion dynamic stabilization on biomechanical responses of the implanted lumbar spine during whole-body vibration. Comput Methods Programs Biomed n.d. Doi: https://doi.org/10.1016/j.cmpb.2020.105441.

[11] Fan W., Guo L-X. The Role of Posterior Screw Fixation in Single-Level Transforaminal Lumbar Interbody Fusion During Whole Body Vibration: A Finite Element Study. World Neurosurg 2018. Doi: 10.1016/j.wneu.2018.03.150.

[12] Fan W., Guo LX., 2021 MZPU-. Biomechanical analysis of lumbar interbody fusion supplemented with various posterior stabilization systems. European Spine Journal n.d. Doi: https://doi.org/10.1007/s00586-021-06856-7.

[13] Fan Y., Zhou S., Xie T., Yu Z., Han X., Zhu L. Topping-off surgery vs posterior lumbar interbody fusion for degenerative lumbar disease: A finite element analysis. J Orthop Surg Res 2019; 14(1). Doi: 10.1186/s13018-019-1503-4.

[14] George SP., Venkatesh K., Saravana Kumar G. Development, calibration and validation of a comprehensive customizable lumbar spine FE model for simulating fusion constructs. Med Eng Phys 2023; 118: 104016. Doi: https://doi.org/10.1016/j.medengphy.2023.104016.

[15] Guo LX., Li R., Zhang M. Biomechanical and fluid flowing characteristics of intervertebral disc of lumbar spine predicted by poroelastic finite element method. Acta Bioeng Biomech 2016; 18(2): 19–29. Doi: 10.5277/ABB-00406-2015-02.

[16] Guo T-M., Lu J., Xing Y-L., Liu G-X., Zhu H-Y., Yang L., Qiao X-M. A 3-Dimensional Finite Element Analysis of Adjacent Segment Disk Degeneration Induced by Transforaminal Lumbar Interbody Fusion After Pedicle Screw Fixation. World Neurosurg 2019; 124: e51–7. Doi: 10.1016/j.wneu.2018.11.195.

[17] Ito K., Ito Z., Nakamura S., Ito F., Shibayama M., Miura Y. Minimization of lumbar interbody fusion by percutaneous full-endoscopic lumbar interbody fusion (PELIF), and its minimally invasiveness comparison with minimally invasive surgery-transforaminal lumbar interbody fusion (MIS-TLIF). Interdisciplinary Neurosurgery 2023; 34: 101794. Doi: 10.1016/j.inat.2023.101794.

[18] Jaramillo HE., Garcia JJ. Elastic constants influence on the L4-L5-S1 annuli fibrosus behavior, a probabilistic finite element analysis. Acta of Bioengineering and Biomechanics Original Paper 2017; 19(4). Doi: 10.5277/ABB-00949-2017-02.

[19] Kim DH., Hwang RW., Lee G-H., Joshi R., Baker KC., Arnold P., Sasso R., Park D., Fischgrund J. Comparing rates of early pedicle screw loosening in posterolateral lumbar fusion with and without transforaminal lumbar interbody fusion. The Spine Journal 2020; 20(9): 1438–45. Doi: 10.1016/j.spinee.2020.04.021.

[20] Lee N., Shin DA., Kim KN., Yoon DH., Ha Y., Shin HC., Yi S. Paradoxical Radiographic Changes of Coflex Interspinous Device with Minimum 2-Year Follow-Up in Lumbar Spinal Stenosis. World Neurosurg 2016; 85: 177–84. Doi: https://doi.org/10.1016/j.wneu.2015.08.069.

[21] Liu Z., Zhang S., Li J., 2022 HTPU-. Biomechanical comparison of different interspinous process devices in the treatment of lumbar spinal stenosis: a finite element analysis. BMC Musculoskelet Disord n.d. Doi: https://doi.org/10.1186/s12891-022-05543-y.

[22] Lo C-C., Lo CC., Tsai KJ., Tsai K-J., Zhong Z-C., Chen S-H., Chen SH., Hung C. Biomechanical differences of Coflex-F and pedicle screw fixation combined with TLIF or ALIF – a finite element study. Comput Methods Biomech Biomed Engin 2011. Doi: 10.1080/10255842.2010.501762.

[23] Lo HJ., Chen HM., Kuo YJ., Yang SW. Effect of different designs of interspinous process devices on the instrumented and adjacent levels after double-level lumbar decompression surgery: A finite element analysis. PLoS One 2020; 15(12 December). Doi: 10.1371/journal.pone.0244571.

[24] Ma X., Lin L., Wang J., Meng L., Zhang X., Miao J. Oblique lateral interbody fusion combined with unilateral versus bilateral posterior fixation in patients with osteoporosis. J Orthop Surg Res 2023; 18(1): 776. Doi: 10.1186/s13018-023-04262-x.

[25] Miękisiak G., Łątka D., Janusz W., Urbański W., Załuski R., Kubaszewski Ł. The change of volume of the lumbar vertebrae along with aging in asymptomatic population: A preliminary analysis. Acta Bioeng Biomech 2018; 20(3): 25–30. Doi: 10.5277/ABB-01166-2018-01.

[26] Mo Z., Li D., Zhang R., Chang M., Yang B., Tang S. Comparative effectiveness and safety of posterior lumbar interbody fusion, Coflex, Wallis, and X-stop for lumbar degenerative diseases: A systematic review and network meta-analysis. Clin Neurol Neurosurg 2018; 172: 74–81. Doi: 10.1016/j.clineuro.2018.06.030.

[27] Nakhli Z., Hatira F Ben., Pithioux M., Chabrand P., Saanouni K. On prediction of the compressive strength and failure patterns of human vertebrae using a quasi-brittle continuum damage finite element model. Acta Bioeng Biomech 2019; 21(2): 143–51. Doi: 10.5277/ABB-01265-2019-03.

[28] Park WM., Li G., Cha T. Development of a novel FE model for investigation of interactions of multi-motion segments of the lumbar spine. Med Eng Phys 2023; 120: 104047. Doi: https://doi.org/10.1016/j.medengphy.2023.104047.

[29] Pradeep K., Pal B. Effects of open and minimally invasive Transforaminal Lumbar Interbody Fusion (TLIF) surgical techniques on mechanical behaviour of fused L3-L4 FSU: A comparative finite element study. Med Eng Phys 2024; 123: 104084. Doi: https://doi.org/10.1016/j.medengphy.2023.104084.

[30] Rana M., Roy S., Biswas P., Biswas SK., Biswas JK. Design and development of a novel expanding flexible rod device (FRD) for stability in the lumbar spine: A finite-element study. Int J Artif Organs 2020; 43(12): 803–10. Doi: 10.1177/0391398820917390.

[31] Salleh NSM., Mazlan MH., Abdullah NS., Ahmad IL., Abdullah AH., Jalil MHA., Takano H., Nordin NDD. Design and analysis of infill density effects on interbody fusion cage construct based on finite element analysis. 1st National Biomedical Engineering Conference, NBEC 2021. Institute of Electrical and Electronics Engineers Inc.; 2021. p. 25–9.

[32] Schenck CD., Terpstra SES., Moojen WA., van Zwet E., Peul W., Arts MP., Vleggeert-Lankamp CLA. Interspinous process device versus conventional decompression for lumbar spinal stenosis: 5-year results of a randomized controlled trial. J Neurosurg Spine 2022; 36(6): 909–17. Doi: 10.3171/2021.8.SPINE21419.

[33] Stokes IAF., Gardner-Morse M. A database of lumbar spinal mechanical behavior for validation of spinal analytical models. J Biomech 2016; 49(5): 780–5. Doi: 10.1016/j.jbiomech.2016.01.035.

[34] Teng L., 2020 YLPU-. Interlaminar stabilization offers greater biomechanical advantage compared to interspinous stabilization after lumbar decompression: a finite element analysis. J Orthop Surg Res n.d. Doi: https://doi.org/10.1186/s13018-020-01812-5.

[35] Teo EC., Ng HW. Evaluation of the role of ligaments, facets and disc nucleus in lower cervical spine under compression and sagittal moments using finite element method. Med Eng Phys 2001; 23(3): 155–64. Doi: https://doi.org/10.1016/S1350-4533(01)00036-4.

[36] Vadapalli S., Sairyo K., Goel VK., Robon M., Biyani A., Khandha A., Ebraheim NA. Biomechanical rationale for using polyetheretherketone (PEEK) spacers for lumbar interbody fusion-A finite element study. Spine (Phila Pa 1976) 2006; 31(26): E992-8. Doi: 10.1097/01.brs.0000250177.84168.ba.

[37] Wang B., Wang B., Wang B., Hua W., Ke W., Lu S., Li X., Zeng X., Yang C. Biomechanical Evaluation of Transforaminal Lumbar Interbody Fusion and Oblique Lumbar Interbody Fusion on the Adjacent Segment: A Finite Element Analysis. World Neurosurg 2019. Doi: 10.1016/j.wneu.2019.02.164.

[38] Wong CE., Hu HT., Kao LH., Liu CJ., Chen KC., Huang KY. Biomechanical feasibility of semi-rigid stabilization and semi-rigid lumbar interbody fusion: a finite element study. BMC Musculoskelet Disord 2022; 23(1). Doi: 10.1186/s12891-021-04958-3.

[39] Xu M., Yang J., Lieberman IH., Haddas R. Finite element method-based study of pedicle screw–bone connection in pullout test and physiological spinal loads. Med Eng Phys 2019; 67: 11–21. Doi: 10.1016/j.medengphy.2019.03.004.

[40] Yan J., Wu Z., Wang X., Xing Z., Song H., Zhao Y., Zhang J., Wang Y., Qiu G. [Finite element analysis on stress change of lumbar spine]. Zhonghua Yi Xue Za Zhi 2009; 89(17): 1162–5.

[41] Yang M., Sun G., Guo S., Zeng C., Yan M., Han Y., Xia D., Zhang J., Li X., Xiang Y., et al. The Biomechanical Study of Extraforaminal Lumbar Interbody Fusion: A Three-Dimensional Finite-Element Analysis. J Healthc Eng 2017; 2017: 9365068. Doi: 10.1155/2017/9365068.

[42] Yang SC., Liu PH., Tu YK. Investigationof pullout strength in different designs of pedicle screws for osteoporotic bone quality usingfinite element analysis. Acta Bioeng Biomech 2019; 21(3). Doi: 10.5277/ABB-01385-2019-03.

[43] Yin J-Y., 2020 LGPU-. Biomechanical analysis of lumbar spine with interbody fusion surgery and U-shaped lumbar interspinous spacers. Comput Methods Biomech Biomed Engin n.d. Doi: https://doi.org/10.1080/10255842.2020.1851368.

[44] Zhao Y., Li J., Wang D., Liu Y., Tan J., Zhang S. Comparison of stability of two kinds of sacro-iliac screws in the fixation of bilateral sacral fractures in a finite element model. Injury 2012; 43(4): 490–4. Doi: 10.1016/j.injury.2011.12.023.

[45] Zhong R., Xue X., Wang R., Dan J., Wang C., Liu D. Safety and efficacy of unilateral and bilateral pedicle screw fixation for lumbar degenerative diseases by transforaminal lumbar interbody fusion: An updated systematic review and meta-analysis. Front Neurol 2022; 13. Doi: 10.3389/fneur.2022.998173.

[46] Zhong Z-C., Wei S-H., Wang J-P., Feng C-K., Chen C-S., Yu C. Finite element analysis of the lumbar spine with a new cage using a topology optimization method. Med Eng Phys 2006; 28(1): 90–8. Doi: https://doi.org/10.1016/j.medengphy.2005.03.007.

[47] Zhu J., Shen H., Cui Y., Fogel GR., Liao Z., Liu W. Biomechanical Evaluation of Transforaminal Lumbar Interbody Fusion with Coflex-F and Pedicle Screw Fixation: Finite Element Analysis of Static and Vibration Conditions. Orthop Surg 2022. Doi: 10.1111/os.13425.

Figure captions.

Figure 1. (a) Intact Lumbar model, (b) Lumbar (L4-L5) surgical model with TLIF implant and Coflex (UCF), (c) Lumbar (L4-L5) surgical model with TLIF implant, Coflex and UPSF (UCF + UPSF), (d) Lumbar (L4-L5) surgical model with TLIF implant, Coflex and BPSF (UCF + BPSF), (e) Intact lumbar model (Meshed View)

Figure 2. (a) Boundary conditions – Intact Model, (b) Angle of rotation of L3 & L4 calculated by ANSYS software. (c) Intact lumbar model deformation plot for four pure moment (10 Nm).

Figure 3. (a) ROM of Intact lumbar spine model (L3-L4) compared with other literature data. (b) Load Vs Displacement of the present FE model (L4 - L5) with Berkson et al.

Figure 4. Comparison of Intact model Mvms (L3-L4) under four pure moment (10 Nm) with literature review data.

Figure 5. Comparison of Surgical mode with Intact model ROM (L3-L4) under four pure moment (7.5 Nm) with follower load (280N).

Figure 6. Comparison of Maximum vonmises stress of : (a) IVD (L3-L4), (b) IVD (L5-S) (c) Implant Cage, (d) Coflex- F IPD

Figure 7. Contour plot of Maximum vonmises stress for: (a) IVD (L3-L4), (b) Implant Cage (c) Coflex- F IPD

Figure 8. (a) Contour plot of Maximum vonmises stress for L4 inferior and L5 superior end plates (b) Comparison of Maximum vonmises stress of L4 inferior end plate (c) Comparison of Maximum vonmises stress of L5 inferior end plate.